JOURNAL OF GEOPHYSICAL RESEARCH, VOL. 115, A04210, doi:10.1029/2009JA014106, 2010

Start-to-end global imaging of a sunward propagating, SAPS-associated giant undulation event

M. G. Henderson,[1] E. F. Donovan,[2] J. C. Foster,[3] I. R. Mann,[4] T. J. Immel,[5] S. B. Mende,[5] and J. B. Sigwarth[6]

Received 27 January 2009; revised 30 July 2009; accepted 19 October 2009; published 22 April 2010.

[1] We present high time resolution global imaging of a sunward propagating giant undulation event from start to finish. The event occurred on 24 November 2001 during a very disturbed storm interval. The giant undulations began to develop at around 1345 UTC and persisted for approximately 2 h. The sunward propagation speed was on the order of 0.6 km/s (relative to magnetic latitude–magnetic local time coordinate system). The undulations had a wavelength of ~718 km and amplitudes of ~890 km and produced ULF pulsations on the ground with a period of ~1108 s. We show (1) that the undulations were associated with subauroral polarization stream (SAPS) flows that were caused by the proton plasma sheet penetrating substantially farther earthward than the electron plasma sheet on the duskside and (2) that they may have been related to the arrival on the duskside of a substorm-associated westward traveling surge-like structure. The observations appear to be consistent with the development of a shear flow and/or ballooning type of instability at the plasmapause driven by intense SAPS-associated shear flows.

Citation: Henderson, M. G., E. F. Donovan, J. C. Foster, I. R. Mann, T. J. Immel, S. B. Mende, and J. B. Sigwarth (2010), Start-to-end global imaging of a sunward propagating, SAPS-associated giant undulation event, *J. Geophys. Res.*, *115*, A04210, doi:10.1029/2009JA014106.

1. Introduction

[2] Large-scale undulations in the equatorward edge of the diffuse aurora were first discovered by *Lui et al.* [1982] in Defense Meteorological Satellite Program (DMSP) photographs. They are predominantly a duskside phenomenon, occurring most commonly in the afternoon to evening local times sectors. They have crest-to-trough amplitudes ranging from 40 to 400 km (or more), wavelengths ranging from about 200 to 900 km, and they tend to occur near the minimum D_{st} of storms during intervals of strong convection. These undulations are not the same thing as Ω bands that are commonly observed to form in the midnight to morning sectors at higher latitudes. Besides the location of occurrence, a major feature that distinguishes the two types of auroral structures is that the "tongues" of auroral luminosity that comprise Ω bands point poleward, while for duskside undulations, they point equatorward.

[3] When the amplitude of the undulations is comparable with their wavelength, the features are referred to as "giant undulations" (GUs). Some examples of these remarkably organized waveforms seen in DMSP imagery during some recent geomagnetic storms are shown in Figure 1. The 27 August 1998 and 17 August 2001 images were taken with the visible operational line scan imager (OLS) on DMSP F13 over the southern polar region. All other images were taken with the OLS imager on DMSP F14 over the northern hemisphere. The K_p value at the time of each image is also shown in Figure 1. Except for the 4 November 2000 event, K_p was 5_0 or above, which is consistent with the giant undulations occurring under high convection conditions.

[4] In order to more clearly place the DMSP GU observations into context, we show in Figure 2, a composite image created by merging the 9 November 1998 DMSP image (shown in Figure 1) into a near simultaneous full-Earth view of the northern auroral distribution as seen by the POLAR/VIS Earth Camera. As shown, the giant undulations during the 9 November 1998 storm occurred in the dusk sector on the equatorward edge of the diffuse aurora and were associated with a large-scale "horn-like" substorm surge structure poleward of the undulations. The poleward surge feature is very commonly observed together with undulations, which suggests that they may be related to storm time substorm activity. It is interesting to note that *Mishin and Mishin* [2007] also find that the arrival of a substorm-associated WTS feature adjacent to the subauroral polarization streams (SAPS) region can lead to the

[1]Los Alamos National Laboratory, Los Alamos, New Mexico, USA.
[2]Department of Physics and Astronomy, University of Calgary, Calgary, Alberta, Canada.
[3]Haystack Observatory, Massachusetts Institute of Technology, Westford, Massachusetts, USA.
[4]Department of Physics, University of Alberta, Edmonton, Alberta, Canada.
[5]Space Sciences Laboratory, University of California, Berkeley, California, USA.
[6]NASA Goddard Space Flight Center, Greenbelt, Maryland, USA.

0148-0227/10/2009JA014106

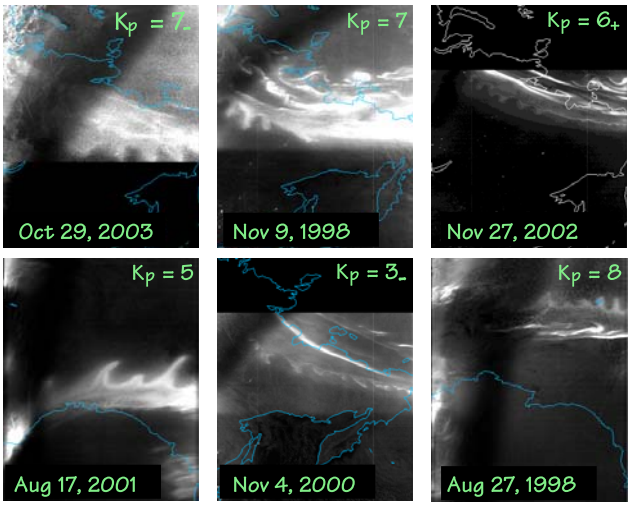

Figure 1. Six recent examples of giant undulations seen in DMSP imagery. The 27 August 1998 and 17 August 2001 images were taken with the visible OLS imager on DMSP F13 over the southern polar region. All other images were taken with the OLS imager on DMSP F14 over the Northern Hemisphere.

production of highly structured and wave-like SAPS. Farther to the east, in the premidnight to morning sector, large-scale auroral streamers are observed and these can often be seen evolving into Ω band structures as shown by *Henderson et al.* [2002].

[5] In the original study of *Lui et al.* [1982], no motion was detected for the undulations because the DMSP imagery is acquired with a scanning-type imager and only a single image is obtained per polar region pass. However, by analyzing successive DMSP images, *Lui et al.* [1982] were able to conclude that the undulations can persist for time periods of 0.5–3.5 h. The first ground-based studies capable of monitoring the development and propagation of the undulations were carried out by *Provadakes et al.* [1989] and *Mendillo et al.* [1989], respectively. However, neither of these studies revealed any systematic motion for the undulations. The first observations of duskside undulations from a snapshot-style space-based global imager were reported by *Murphree and Johnson* [1996] using data from the Freja spacecraft. As with the previous ground-based observations, they detected no systematic azimuthal motion of the waveforms. However, although the Freja imager was capable of 6 s temporal resolution, it acquired images in sets of three, with each set separated widely in time, and therefore, viewing conditions. In other words, the undulations in the *Murphree and Johnson* [1996] study were seen with very high temporal resolution, but also over a very brief span of time. Their results, therefore, indicate that if the waveforms propagated at all, they did not propagate very fast.

[6] The first observations indicating that duskside undulation waveforms can propagate were presented by *Nishitani et al.* [1994]. They reported a duskward phase speed of 540–650 m/s together with a strong latitudinal velocity shear during the 22 min period of observation. More recently, *Baishev et al.* [2000] have presented ground-based observations showing a duskward phase speed of ~700 m/s for undulations that began ~40 min after a substorm onset and persisted for ~80 min. *Baishev et al.* [2000] also reported that the undulations were accompanied by the occurrence of Pc5 magnetic pulsations on the ground.

[7] The excitation mechanism for duskside undulations at the equatorward edge of the diffuse aurora is not yet completely understood, but there is substantial evidence to suggest that they are at least partially driven by an intense latitudinal velocity shear on the duskside. In their original study, *Lui et al.* [1982] proposed that the undulations could be Kelvin-Helmholtz waves driven by the velocity shear between the corotating plasmasphere (tailward flow on the duskside) and the mean plasma sheet flow (sunward on the duskside). However, using the combined shear flow ballooning instability analysis of *Vinas and Madden* [1986], *Kelley* [1986] showed that the nominal shear at the plasmasphere–plasma sheet interface is far too small for instability to occur. Furthermore, large-scale duskside undulations are not observed all the time. They are typically observed only near the peak of geomagnetic storms and there is some evidence to suggest that they may be related to storm time substorm activity. Thus, instead of the nominal duskside plasmasphere–plasma sheet velocity shear, *Kelley* [1986] suggested that the undulations could be driven by the much larger velocity shear associated with storm time "subauroral ion drift" events (SAIDs) or "polarization jets" (PJs) in which the hot ring current protons penetrate substantially further equatorward than the electrons during magnetic storms and/or intense storm time substorms. (Note that in more recent literature, the terms SAID and PJ have been subsumed with the more inclusive terminology of "SAPS" [*Foster and Burke*, 2002].)

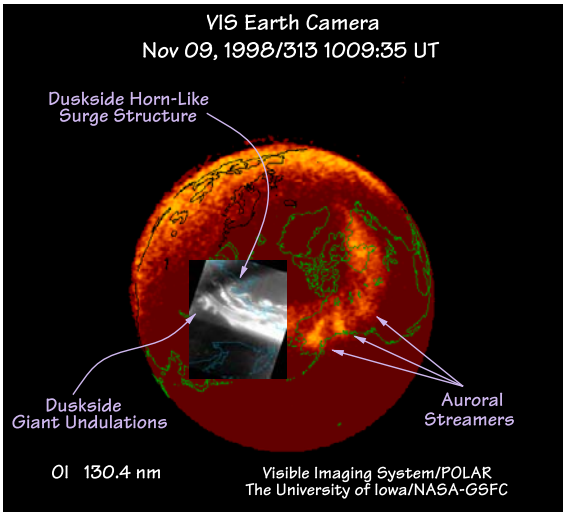

Figure 2. Composite of a high-resolution visible DMSP-F14/OLS image and a POLAR/VIS 130.4 nm Earth Camera image. Undulations on the equatorward edge of the diffuse aurora occur on the duskside and are frequently associated with a higher latitude horn-like surge structure. Streamers and Ω bands tend to occur in the midnight-to-morning sectors at higher latitudes.

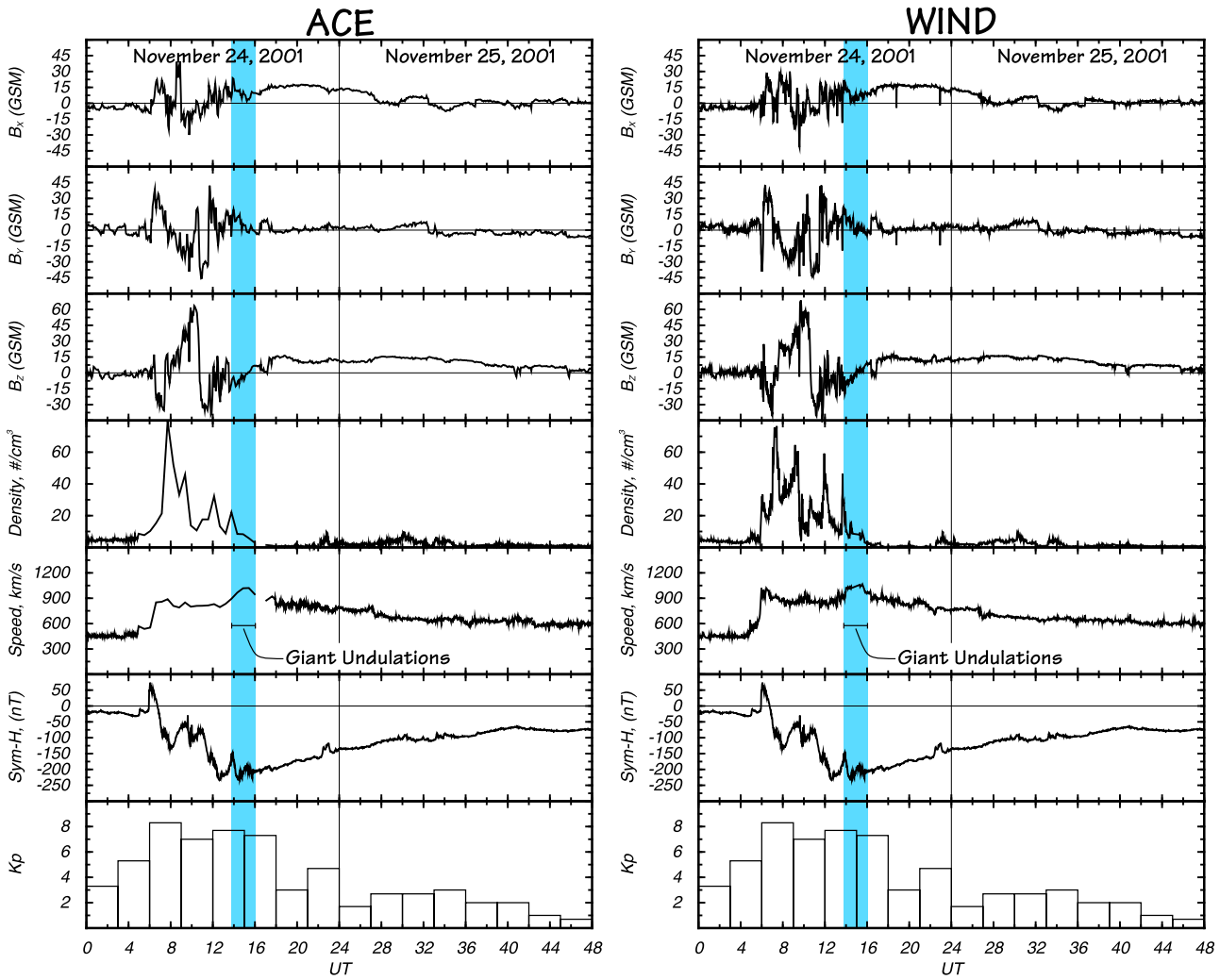

Figure 3. Interplanetary magnetic field and solar wind data from the ACE and WIND spacecraft together with the Sym-H index. Between approximately 0600 and 1600 UTC on 24 November, the 64 s resolution ACE solar wind data are unavailable because of problems associated with solar energetic proton background contamination; 30 min samples are shown instead.

[8] Other more recent studies that may be relevant to the topic of giant undulations also exist. *Goldstein et al.* [2005] examined the possibility that westward moving ripples on the plasmapause could be generated as a result of substorm injections. *Mishin and Burke* [2005] also found that substorm-associated SAPS can become highly structured and wave-like following the onset of storm time substorms. *Mishin and Mishin* [2007] showed that the start of highly structured SAPS was coincident with the arrival of a westward traveling surge adjacent to the SAPS region. Others [e.g., *Lin et al.*, 2007] have shown that very strong shear flows can exist near the plasmaspheric plume boundaries.

[9] Although a number of high time resolution global auroral imagers have flown over the past 20 years, to date no global imaging of an entire giant undulation event from start to finish has been reported in the literature. The most likely reason for this is that the global imagers flown so far have had insufficient spatial resolution to see all but the largest giant undulation events, and those events are relatively rare. In this paper, we present observations of just such an event that we were lucky enough to capture with the IMAGE/FUV imager. The event occurred following a large substorm on 24 November 2001 during a very disturbed storm interval and represents the first ever high time resolution global auroral imaging of a sunward propagating giant undulation event from start to finish.

2. Observations

[10] Interplanetary magnetic field (IMF) and solar wind (SW) data from the ACE and WIND spacecraft for 24–25 November 2001 are presented in Figure 3 together with the 1 min resolution Sym-H and 3 h K_p indices. The first, second, and third panels show the IMF B_x, B_y, and B_z components in GSM coordinates. The fourth and fifth panels show the solar wind proton density and speed, and the sixth and seventh panels show the Sym-H and K_p indices. For ACE, the IMF values are 4 min averages and the solar wind values are nominally 64 s averages. However, between approximately 0600 and 1600 universal time coordinated

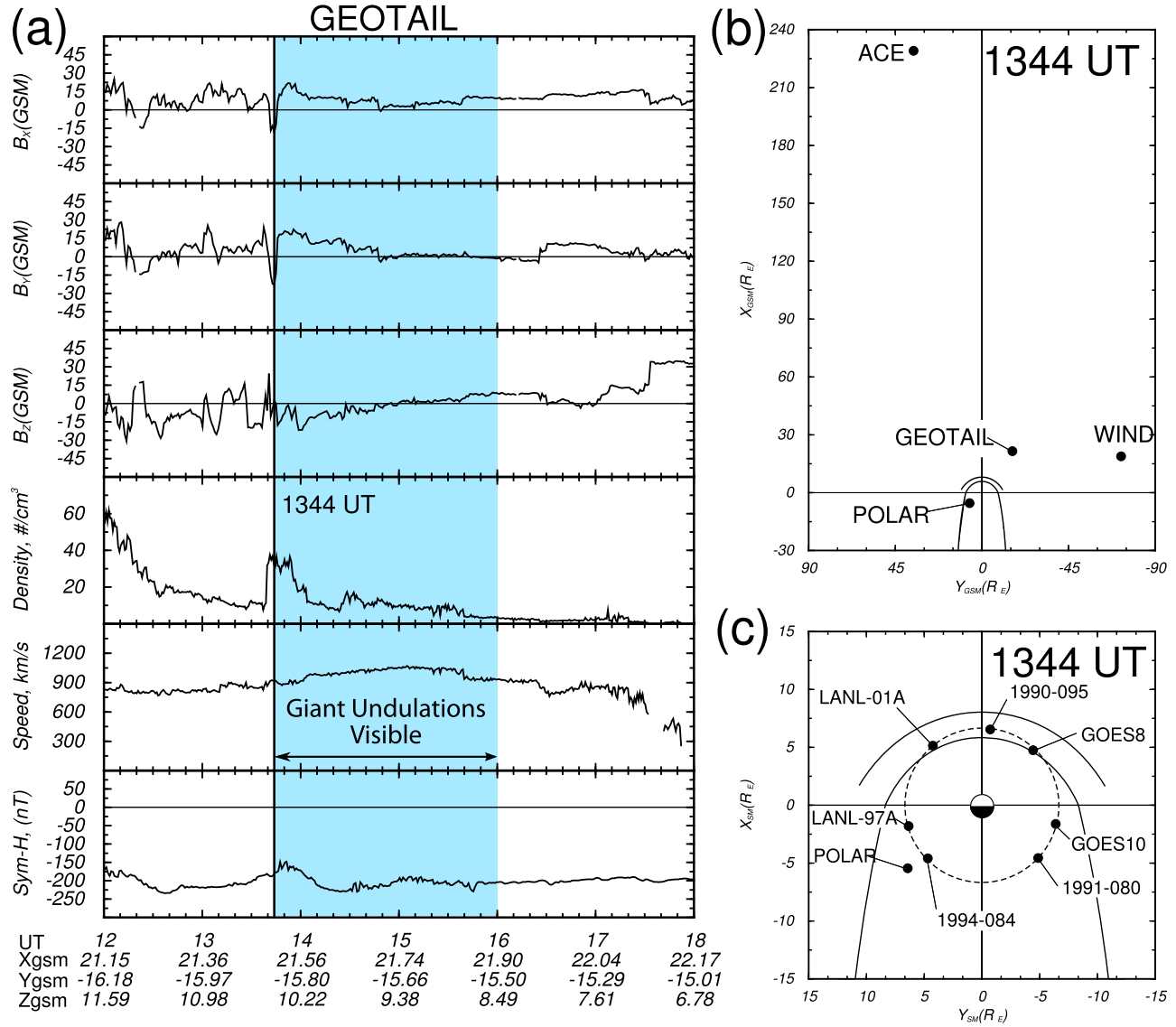

Figure 4. (a) Interplanetary magnetic field and solar wind data from the GEOTAIL spacecraft together with the Sym-H index. (b) Locations of ACE, WIND, GEOTAIL, and POLAR in GSM coordinates relative to the (model) magnetopause at 1344 UTC. (c) Locations of POLAR, GOES-8, GOES-10, and the LANL-instrumented spacecraft: 1990–095, 1991–080, 1994–084, LANL-01A, and LANL-02A relative to the (model) magnetopause at 1344 UTC.

(UTC) on 24 November, the 64 s solar wind data were unavailable because of the contamination by a solar energetic proton event. Reliable data were available only every half hour during this period when the ACE/SWEPAM instrument performed full energy sweeps. The time resolution for the WIND data is 1 min for the IMF and ~100 s for the solar wind. The ~2 h time period during which the giant undulations were seen on 24 November 2001 are highlighted on both the ACE and the WIND plots. During this time period, ACE and WIND were situated at approximately (229, 37, −20) R_E and (19, −74, 28) R_E, respectively, in GSM coordinates. In order to more accurately specify the solar wind structures that actually impinged upon the Earth, we have applied a nominal 0.5 h time shift to the ACE data. This is consistent with a solar wind speed of approximately 811 km/s, which is close to the observed speed near the time that the giant undulations were observed. No time shift was applied to the WIND data because it was already fairly close to the Earth's magnetopause during this event.

[11] From Figure 3, we can see that the IMF and solar wind were highly disturbed on 24 November with B_z reaching values greater than 60 nT (63.5 nT at the delayed time of 1014 UTC) and less than −39 nT (−39.6 nT at the delayed time of 1150 UTC), and the proton density reaching values in excess of 79 cm^{-3} (79.67 cm^{-3} at a delayed time of ~0742:53 UTC). These disturbed conditions develop abruptly following the arrival of a shock near 0600 UTC and persist until about 1600 UTC. By ~1800 UTC, the IMF B_z turns positive and remains that way for more than a day. The IMF and SW data from both ACE and WIND appear to be consistent with the arrival of a coronal mass ejection (CME)-induced magnetic cloud over the Earth. The cloud itself

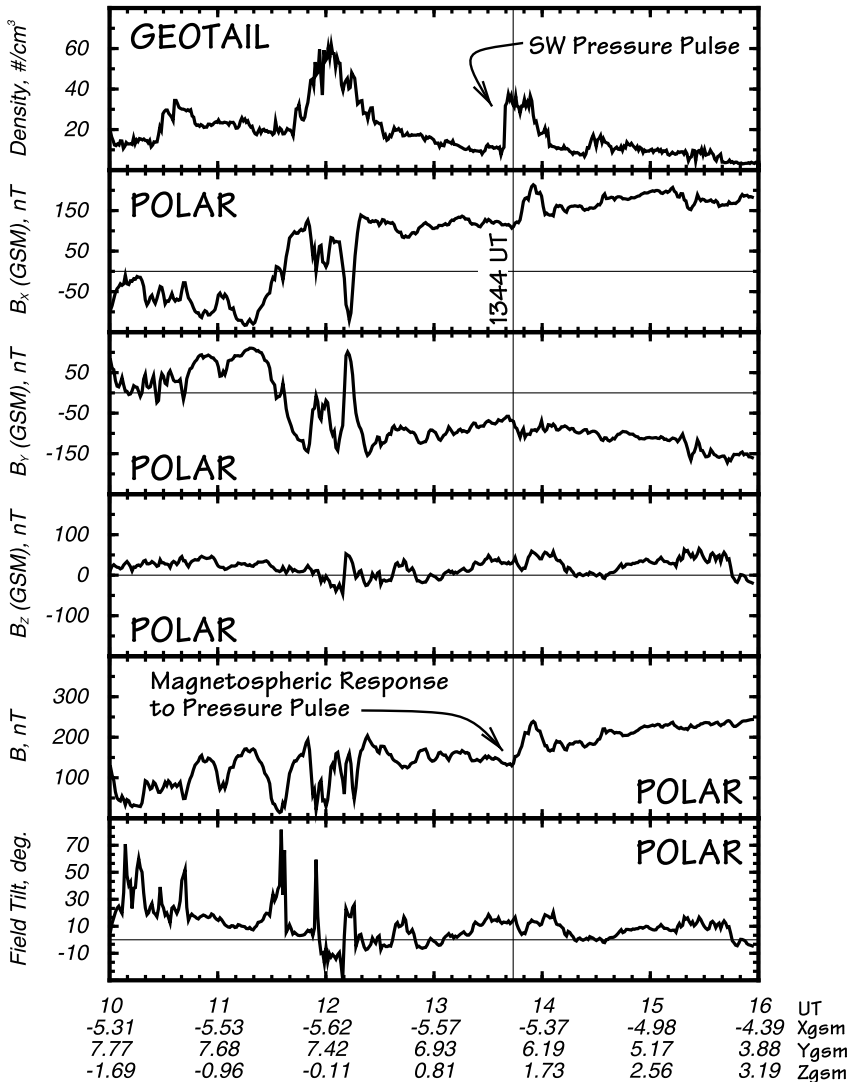

Figure 5. Magnetic field behavior at POLAR together with the solar wind density as measured just upstream of the bow shock by GEOTAIL. The nightside magnetospheric response (at POLAR) to the pressure pulse can be seen as an abrupt increase in the magnitude of $\vec{B}$ at 1344 UTC.

arrived at around 1600 UTC following a compressed upstream sheath-like region between about 0600 and 1600 UTC. During the sheath interval, the proton density is highly structured, which gives rise to several strong pressure pulses between 06 and 1600 UTC on 24 November. One of these pressure pulses (1341 UTC in the WIND data) occurs just prior to the development of the giant undulations.

[12] The Sym-H index shown in Figure 3 indicates that the arrival of the CME-driven disturbance produced a strong storm, the minimum value of Sym-H was −234 nT at 1237 UTC on 24 November 2001. Much of the structure in Sym-H during the main phase is because of the large fluctuations in the solar wind dynamic pressure which are not corrected for in Sym-H. In agreement with prior studies, we also find that the giant undulations appear near the peak of the storm as measured by Sym-H and during a time of strong convection as indicated by the high value of the K_p index (8- between 1200 and 1500 UTC).

[13] IMF and SW data are also available from the GEOTAIL spacecraft as shown in Figure 4a. The locations of GEOTAIL, ACE, WIND, POLAR, GOES 8/10, and five of the LANL geosynchronous satellites, at 1344 UTC, are shown in Figures 4b and 4c together with a model magnetopause. As can be seen, GEOTAIL was much closer to the magnetosphere than either ACE or WIND, and therefore, provides a more direct monitor of the IMF/SW disturbances that actually hit the Earth's magnetosphere. The data in Figure 4a are not time shifted, but the delay times between GEOTAIL and the magnetopause are estimated to be only about 2–3 min. Note that the large pressure pulse seen at ACE and WIND (Figure 3) prior to the formation of the giant undulations at 1344 UTC was also observed at GEOTAIL prior to 1344 UTC.

[14] The magnetospheric response to this pressure pulse at the location of the POLAR spacecraft (which was situated in the dusk to midnight sector) can be seen in Figure 5. The first panel shows the GEOTAIL SW proton density, while the second through sixth panels show the magnetic field behavior at POLAR in GSM coordinates (B_x, B_y, B_z, $|B|$, and

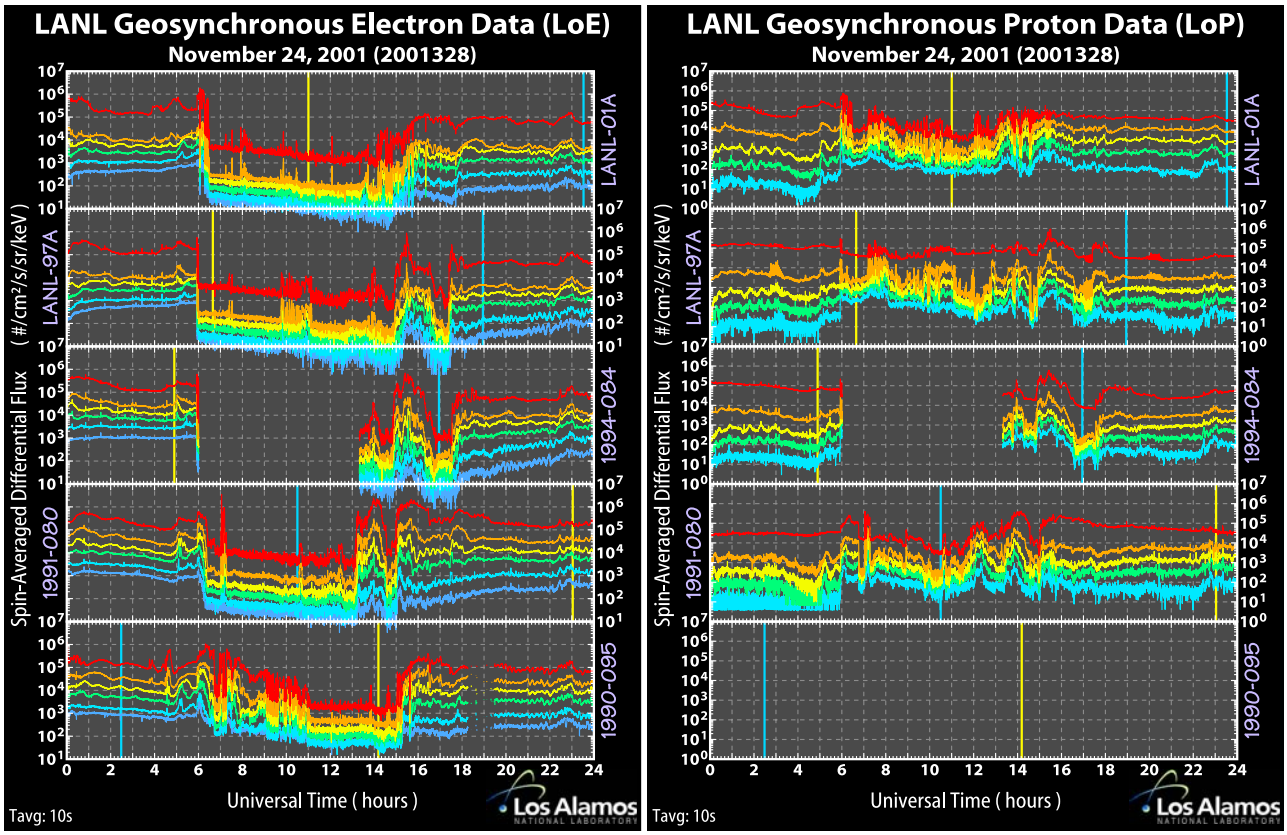

Figure 6. LANL geosynchronous energetic electron and proton fluxes on 24 November 2001. Yellow and blue vertical lines indicate when a spacecraft passes through magnetic local noon and midnight, respectively.

field inclination angle, defined to be $\tan^{-1}(B_z/\sqrt{B_x^2 + B_y^2})$. As can be seen, the nightside magnetospheric response (at POLAR) to the pressure pulse is an abrupt increase in the field strength at 1344 UTC, which was also associated with a small decrease in the field inclination angle. Thus, the pressure pulse arrived at the location of POLAR (in the dusk-to-midnight sector) at about the same time that the giant undulations formed.

[15] Energetic electron and proton data on 24 November 2001 from the Los Alamos National Laboratory (LANL) geosynchronous particle detectors are presented in Figure 6. Data from five spacecraft distributed around the Earth are shown at 10 s resolution. The yellow and blue vertical lines show the universal time when each spacecraft passed through 12 and 24 MLT, respectively. Because of noise problems, proton data are unavailable from 1990–095. The electron data show strong flux dropouts at all spacecraft following the arrival of the shock at around 0600 UTC. This is true not only for the spacecraft situated on the dayside, but also for those on the nightside. These observations are consistent with the dayside magnetopause being pushed inside of geosynchronous orbit between 0600 and 1300 UTC because of the large dynamic pressure (and high negative IMF B_z values) in the solar wind during that time period. In addition, the nightside flux dropouts indicate that the nightside portion of geosynchronous orbit resided in the lobe for much of the same time period and that the nightside magnetic field must have been very highly stretched which is consistent with the polar observation.

[16] An overview of the northern auroral distribution as seen by the IMAGE/FUV WIC instrument is shown in Figure 7. Images are shown approximately every half hour over the time period between 0933 and 1430 UTC. In the first three frames, a large patch of luminosity can be seen extending poleward from the nominal oval latitudes near noon and appears to be associated with transpolar arcs and regions of enhanced luminosity within the polar cap regions. This feature is probably associated with the cusp. In addition, an auroral structure can be seen extending equatorward and westward away from the postnoon sector. This type of configuration has been observed before with IMAGE/FUV and has been dubbed the "Q-aurora" [*Immel et al.*, 2002; *Fuselier et al.*, 2002]. Between 1100 and 1330 UTC, the cusp and "Q" features have faded away and the auroral forms in the polar cap are being swept toward the dawnside. Also during this time period, substorm-like intensifications can be seen on the nightside of the auroral distribution; although in this overview plot, much of this activity is saturated because of the scaling of the data. The giant undulations are first seen in the FUV WIC image taken at 1345:18 UTC and seem to have been preceded by a substorm. The last two frames in Figure 7 show well-developed giant undulations in the equatorward edge of the diffuse aurora in the dusk-to-noon sector.

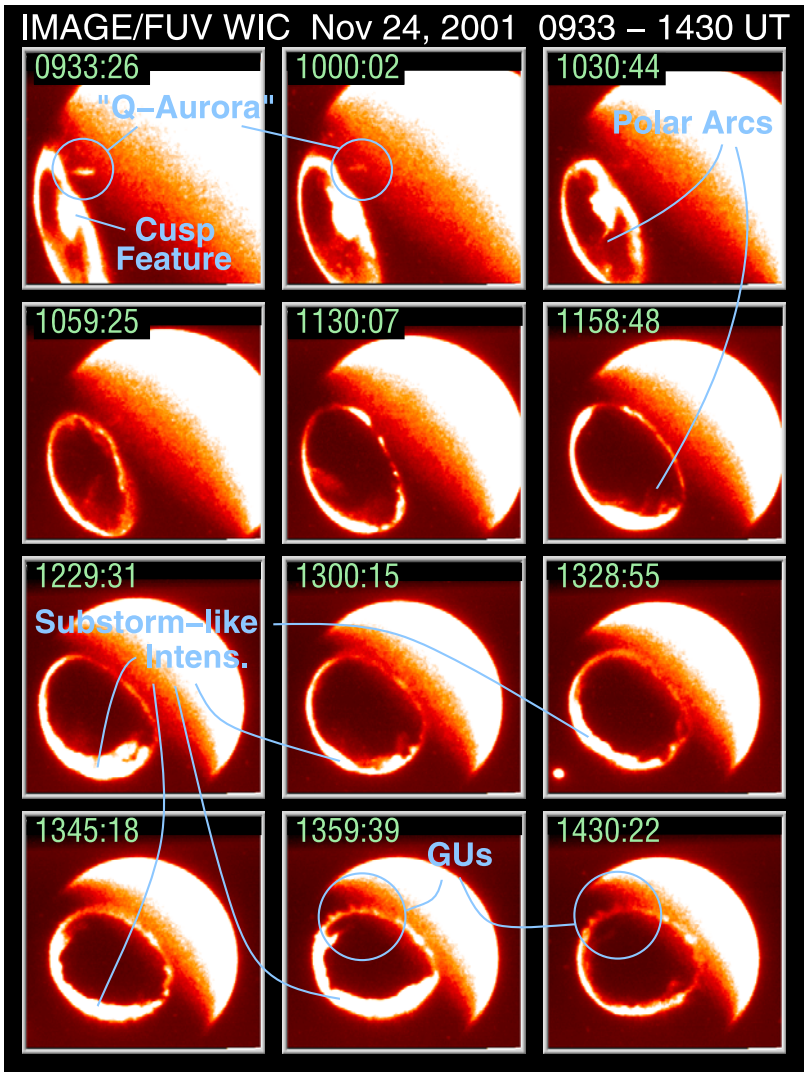

Figure 7. Overview of the northern auroral distribution as seen by IMAGE/FUV WIC. Images are shown approximately every half hour over the time period between 0933 and 1430 UTC. A large cusp-related protrusion of the auroral emission can be seen in the first three images.

[17] In Figure 8, we present IMAGE/FUV WIC images acquired during an approximately 1 h period preceding the development of the giant undulations. For this sequence, every second image is shown and the scaling of the data has been adjusted in order to enhance detail associated with the substorm-like activity on the nightside. At 1252:03 UTC, a localized region near midnight brightens and subsequently expands poleward eastward and westward. The first frame from IMAGE/FUV in which the giant undulations are clearly seen was taken at 1345:30 UTC; although the frame taken at 1343:27 UTC (not shown) also appears to show some periodic structuring of the dusk-to-noon auroral distribution. The giant undulations appear to develop when the westward expanding substorm-associated auroral forms reach the dusk sector. However, the frame at 1345:30 UTC also shows the start of a sudden brightening across the entire dayside oval indicating the arrival of the large pressure pulse observed in Figure 3.

[18] A more detailed view of the giant undulations, particularly around the time of their development is presented in Figure 9. All available images taken between 1341:13 and 1351:27 UTC are shown in the first six frames (they were taken about 2 min apart). From 1401:42 UTC onward, images taken approximately 10 min apart are presented (although we note that an image is available every 2 min spin period throughout the entire event). In the image taken at 1345:18 UTC, the entire dayside portion of the auroral distribution begins to brighten and by the time of the next image, at 1347:21 UTC, it is nearly as bright as the nightside oval. As noted earlier, this is likely the time at which the large pressure pulse observed at ACE and WIND apparently hit the magnetosphere. Since the giant undulations are also first seen in the FUV data in the image taken at 1345:18 UTC, it is not clear whether their development was triggered by the pressure pulse or by the arrival, at dusk, of the westward expanding substorm-associated disturbance.

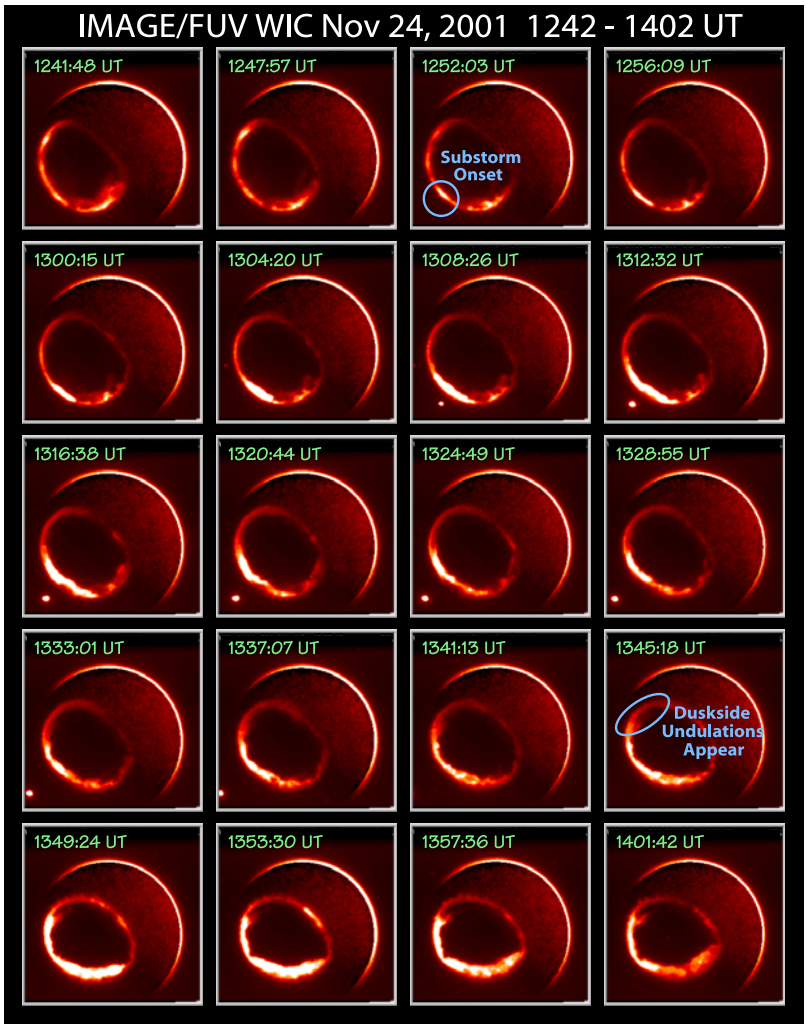

Figure 8. Sequence of IMAGE/FUV WIC images during the hour preceding the formation of the giant undulations. The scaling of the images is optimized for viewing the intense substorm-like activity observed on the nightside and is therefore not well suited for observing the giant undulations which develop at around 1345 UTC.

[19] In Figure 10a, we present a set of images showing the rate at which a given undulation moves sunward. All four images are presented in magnetic coordinates with 12 MLT up and 18 MLT to the left in each image. The annotated blue dashed line shows the MLT position of the undulation as a function of time. Between 1413:59 UTC and 1454:57 UTC the undulation had an average azimuthal speed of 9.886×10^{-3} °/s that translates to about 0.6 km/s at a latitude of 55°. Note that this speed is relative to an MLAT-MLT coordinate system, not to the surface of the Earth. If we take into account the angular velocity of the Earth, the waves move with a speed of approximately 0.9 km/s relative to the Earth's surface. Figure 10b also shows that the wavelength (at a latitude of 55°) and amplitude of the undulations are approximately 718 and 890 km, respectively.

[20] In Figure 11, we present a sequence of images acquired with the POLAR/VIS instrument. The "full-Earth" images in Figure 11 (left) were taken with the Earth Camera (EC), which is sensitive to a broad range of FUV wavelengths around the OI (130.4 nm) emissions. The images in Figures 11 (middle) and 11 (right) were taken with the low resolution camera (LRC). Despite its name, the VIS/LRC provides much higher resolution images than the Earth Camera does. Figure 11 (middle) shows the N_2^+ (391.4 nm) emissions, while Figure 11 (right) shows the OI (630.0 nm) red line emissions. The giant undulations can be seen clearly on the duskside of the northern auroral distribution in the EC images. However, they cannot be seen in the LRC images because these higher resolution images have a smaller field of view that is centered on the auroral distribution in the pre-midnight-to-midnight sector (i.e., the LRC was not looking at the dusk sector). Nevertheless, the LRC images show an interesting feature in the equatorward regions of the auroral oval in the premidnight sector. A comparison of the four sets of 391.4 and 630.0 nm images shown in Figure 11 indicates that the equatorward edge of the oval extends to much lower latitudes in the 630.0 nm images. This is probably a result of proton precipitation extending to lower latitudes than does the region of electron precipitation. As pointed out by *Lummerzheim et al.* [2001] precipitating protons can easily

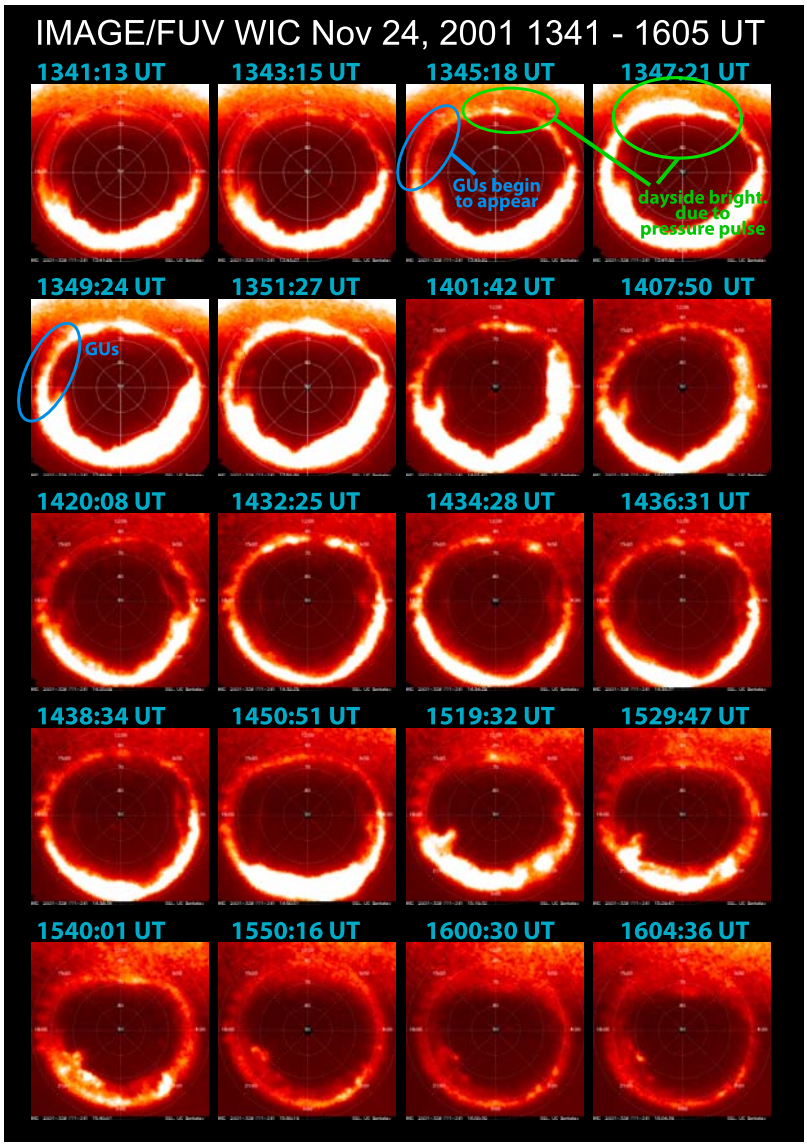

Figure 9. Sequence of IMAGE/FUV WIC images spanning the time during which the giant undulations were observed. The images have been reprojected into a magnetic coordinate system in which local magnetic noon is at the top and local magnetic dusk is to the left in each image. The latitude circles are drawn every 10°. The scaling of the data was optimized for viewing the giant undulations, which unfortunately saturates the more intense substorm-like emissions on the nightside. The GUs are first seen in the 1345:18 UTC image. This time appears to be coincident with the arrival of a pressure pulse that manifests itself in the images as a broadly distributed brightening of the dayside auroral distribution.

excite OI (630.0 nm) emissions but not N_2^+ (391.4 nm) emissions. This is because the secondary electrons produced by proton precipitation are too low in energy to cause additional excitations needed to produce N_2^+ (391.4 nm) emissions but can much more easily produce OI (630.0 nm) emissions because of this state's low excitation potential. Thus, the differences seen in the N_2^+ (391.4 nm) and OI (630.0 nm) images are likely because of protons penetrating much closer to the Earth than the electrons can in the inner magnetosphere. This type of configuration in the magnetosphere is thought to be a driver for SAPS in the afternoon-to-midnight sectors.

[21] In Figure 12a, we present a sequence of images acquired with the optical line scan (OLS) visible light imager on the DMSP F13, F14, and F15 spacecraft during successive passes of the northern polar region. It is important to note that these images are not snapshots. Instead, they are scanned row by row as the spacecraft moves in its orbit. This mode of imaging results in extremely high spatial resolution but unfortunately each row of an image is acquired at a different time which can lead to a distorted view of rapidly changing scenes. The time shown on each of the strip images in Figure 12 corresponds to the approximate time at which the equatorward edge of the auroral distribution (horizontally at the center of each image) was scanned.

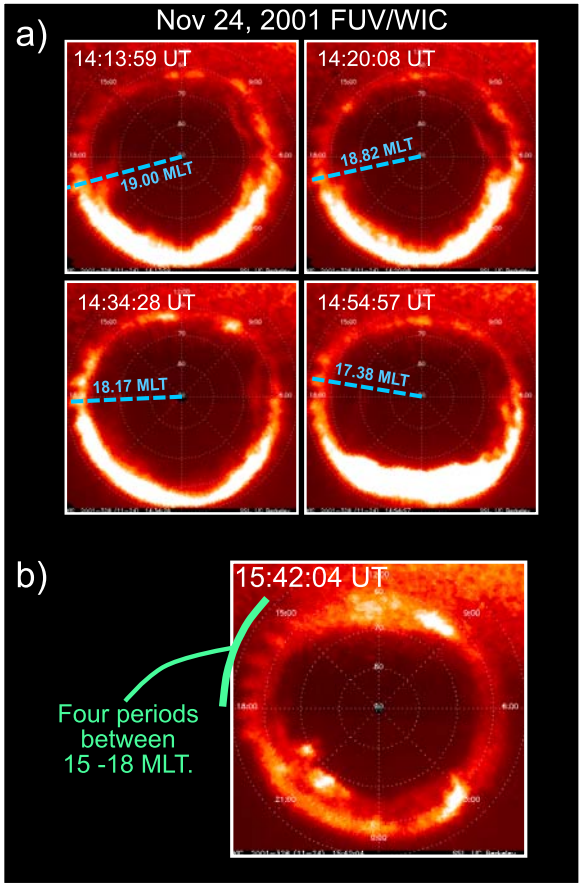

Figure 10. (a) Set of four IMAGE/FUV WIC images highlighting the sunward azimuthal motion of the giant undulations. The raw images have been reprojected into a magnetic coordinate system in which magnetic local noon (top) and magnetic local dusk (left) are shown. The undulations are visible on the duskside between magnetic latitudes of ~50° and ~60° and have amplitudes of approximately 8° (corresponding to ~890 km). The undulation highlighted with the blue dashed line moved approximately 1.62 h of MLT in 2458 s. At a latitude of 55°, this translates into a sunward speed of approximately 0.6 km/s. (b) IMAGE/FUV WIC image taken at 1542:04 UTC showing five undulations (four wavelengths) spanning the local time sector between 15 and 18 MLT. The wavelength is approximately 0.75 h of MLT, which corresponds to about 718 km at a latitude of 55°.

[22] At 1201 UTC, the DMSP imagery shows no evidence of undulations at the equatorward edge. However, by 1316 UTC, the equatorward edge clearly displays some small-amplitude undulations over central Russia as well as what appears to be the leading tip of a surge-like structure at higher latitudes extending in to the field of view from the east. By 1340 UTC, giant undulations are clearly seen on the equatorward boundary of the oval between western Russia and Scandinavia and these undulations persist in the DMSP imagery up until at least 1525 UTC as seen in the sixth frame in Figure 12a. In Figures 12b and 12c, we show an IMAGE FUV/WIC image taken at 1519:32 UTC with the 1525 UTC DMSP/F13 OLS image overlaid (note that the images are merely pasted together and the relative positioning of the data is only qualitatively accurate). The city lights from Oulu, Moscow, St. Petersburg, and Helsinki are highlighted with arrows in Figure 12c. From this composite image, we see that the DMSP image from F13 at 1525 UTC captured the easternmost crests of the giant undulation wave train which, in the FUV/WIC image are seen extending farther to the west toward Greenland.

[23] From Figure 12c, we can see that the sunward moving giant undulations swept directly across England. In Figure 12d, we present magnetometer data from York, which is part of the subauroral magnetometer network (SAMNET) magnetometer array (the *HDZ* coordinate system has *H* horizontal to the ground and pointing toward the magnetic north, *Z* pointing down, and *D* toward the east). The *H*, *D*, and *Z* traces all show large-amplitude continuous-type pulsations with a periodicity of approximately 1108 s (approximately 0.90 mHz) that puts them in the very long period Pc6 category. The pulsations were most prominent in the York magnetometer station, but were also seen at other stations in the SAMNET array as well. We also note that, because of the rotation of the Earth, the 1108 s period seen on the ground is somewhat shorter than the period that would be seen in a fixed inertial frame (because the waves travel in a direction opposite to the rotation of the Earth).

[24] In Figure 13a, we present further evidence that a strong SAPS feature was present on the duskside during this event. Shown are DMSP/F13 plasma and magnetic field measurements acquired between 1515 UTC and 1531 UTC. At the start of this time period, DMSP/F13 was at low latitudes (25.5° MLAT) in the dusk sector (18.1 MLT) and was moving poleward. The trajectory of the spacecraft in geographic coordinates is shown in Figure 13b and relative to the auroral undulations, the trajectory can be inferred from the sixth image shown in Figure 12a (the spacecraft moved poleward (vertically) along the center of the image across Scandinavia). From Figure 13a, we can see that the equatorward edge of the electron precipitation region was encountered at approximately 59.0° MLAT. However, the drift meter measurements (purple curve in the fifth panel) shows that a pronounced sunward convection (poleward electric field) extends to much lower latitudes. This SAPS feature has a peak sunward flow of ~1500 m/s near 50° MLAT and has a "background" flow velocity of ~1000 m/s (westward).

[25] A GPS-derived total electron content (TEC) map [*Coster et al.*, 2003] over Europe near 1520 UTC is shown in Figure 13b. Here, the colors display units of log10 TECu (i.e., 1×10^{16} electrons/mm^2) and the TEC image comprises about 10 min of observations. The location adopted for each pixel is the geographic location of the assumed 350 km altitude piercing point [e.g., *Rideout and Foster*, 2005]. Note that 350 km is somewhat higher than where the auroral emissions occur (which is closer to 100–120 km). In addition, the DMSP data and trajectory in this figure have not been mapped down to the assumed 350 km piercing height. However, we have verified that the actual geographic footprints of DMSP (at 350 km altitude) are shifted poleward by only approximately 1°–2° at most and the longitude of the footprint is shifted by less than 1/4 of a degree. Since the errors in mapping are smaller than the pixel sizes in the TEC map, and because we are interested in making a qualitative comparison between the DMSP and TEC mea-

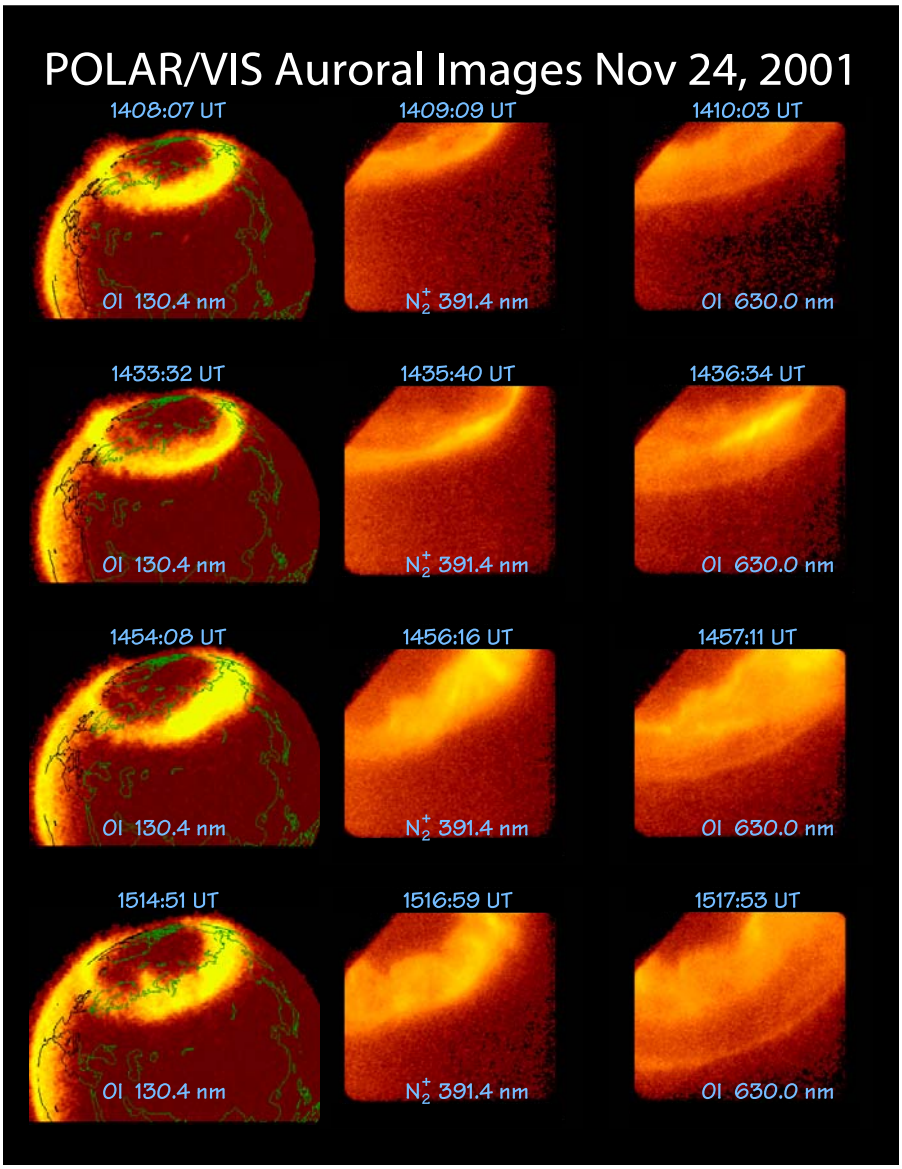

Figure 11. Sequence of POLAR/VIS images spanning the time during which the giant undulations were observed. (left) The GUs can be seen in the "full-Earth" 130.4 nm images from the EC). Emission from the LRC: (middle) 391.4 mm and (right) 630.0 nm. Although the GUs were located outside (to the west) of the field of view of the LRC, the images show clear evidence of a large separation between the proton and electron precipitation regions in the premidnight sector. These conditions are thought to drive SAPS.

surements, we will ignore the small uncertainties associated with mapping for now. A more accurate comparison between the DMSP flow measurements and the FUV auroral measurements will be presented later in Figure 14c, where we actually map the DMSP data down to typical auroral altitudes.

[26] The DMSP/F13 trajectory (in geodetic geographic coordinates) is plotted on top of the map in Figure 13b and the drift meter horizontal velocity and density measurements are replotted vertically to the left of the map as a function of geodetic latitude. As can be seen, a patchy, structured band of elevated TEC lies across Scandinavia at the poleward extent of a deep trough which marks the peak of the SAPS electric field. The latitudinal extent of the TEC band is very close to that of the imaged giant undulation features seen in Figure 12a (sixth frame). In addition, there is a topside density enhancement associated with a narrow region of ion and soft electron precipitation at the equatorward edge of the auroral precipitation region which lies near 61°N MLAT as can be seen in Figure 13a. If we assume that the TEC boundaries identify the location of the plasmapause [e.g., *Foster et al.*, 2002], then these observations indicate that the giant undulations reside just poleward of the plasmapause and are associated with an azimuthally organized spatial structuring of the density.

[27] To further place the giant undulation observations into context, we show the 1525:41 UTC FUV/WIC image in Apex magnetic coordinates in Figure 14a. We have also mapped this same image to the equatorial plane of the solar magnetic (SM) coordinate system as shown in Figure 14b.

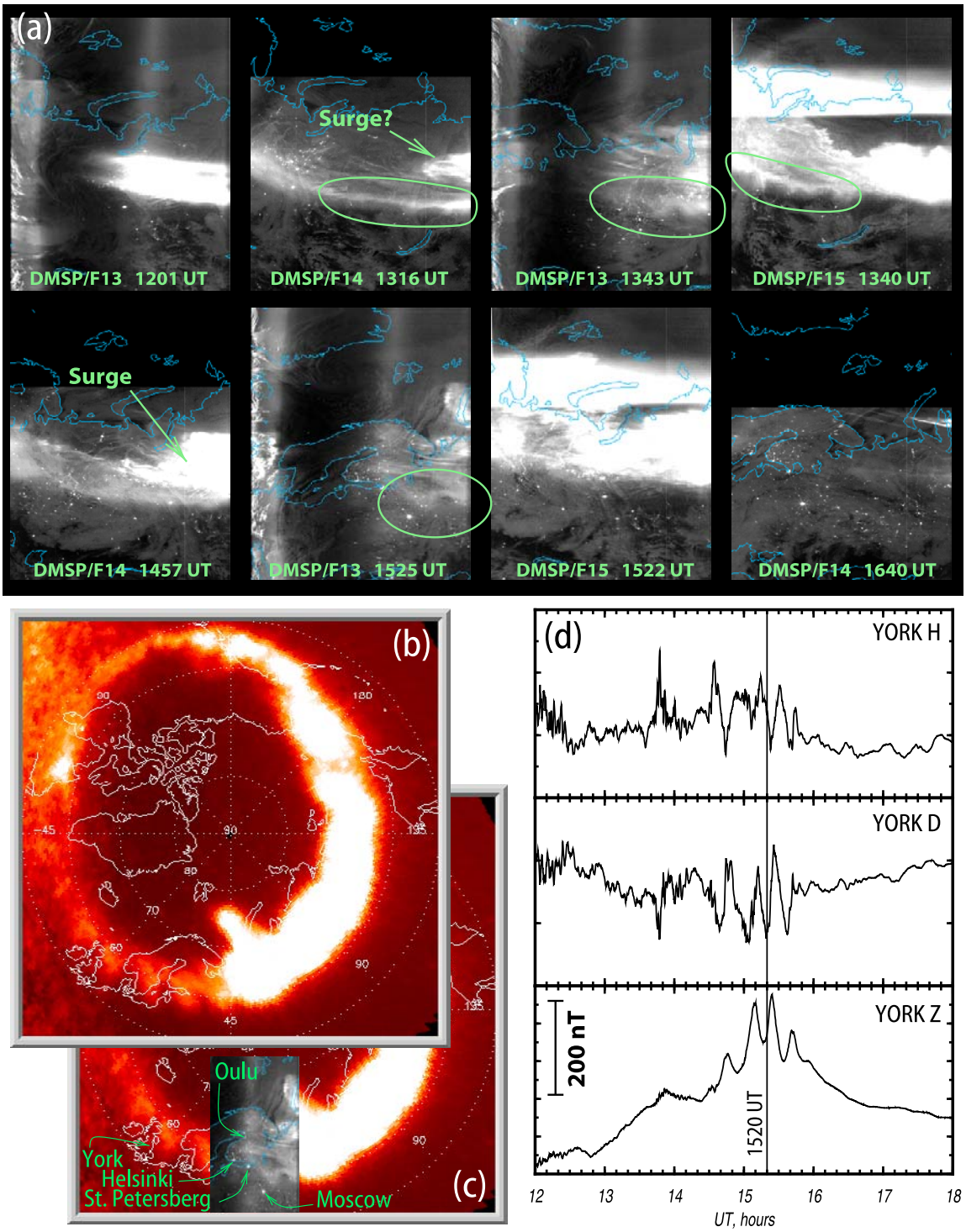

Figure 12. (a) A sequence of DMSP/OLS images acquired during overflights of the undulation region. (b) IMAGE/FUV image taken at 1519:32 UTC. (c) IMAGE/FUV and DMSP/OLS composite image. The undulations in the DMSP visible light image were scanned at approximately 1525 UTC. For reference, the city lights of Oulu, Helsinki, St. Petersburg, and Moscow are highlighted in the DMSP image. (d) Magnetometer traces from YORK (which is part of the SAMNET magnetometer array) show clear large ULF pulsations in the Pc5 range associated with the passage of the undulations overhead.

The magnetic field model used for the mapping in Figure 14b and to compute the Apex magnetic coordinates in Figure 14a is the Tsyganenko storm time magnetic field model, TS04 [*Tsyganenko and Sitnov*, 2005]. The model is dynamic and requires as input, the IMF, SW, and D_{st} time histories since the start of the storm. In Apex coordinates, lines of constant latitude represent features threading field lines that map to constant apex heights (maximum distance from Earth along

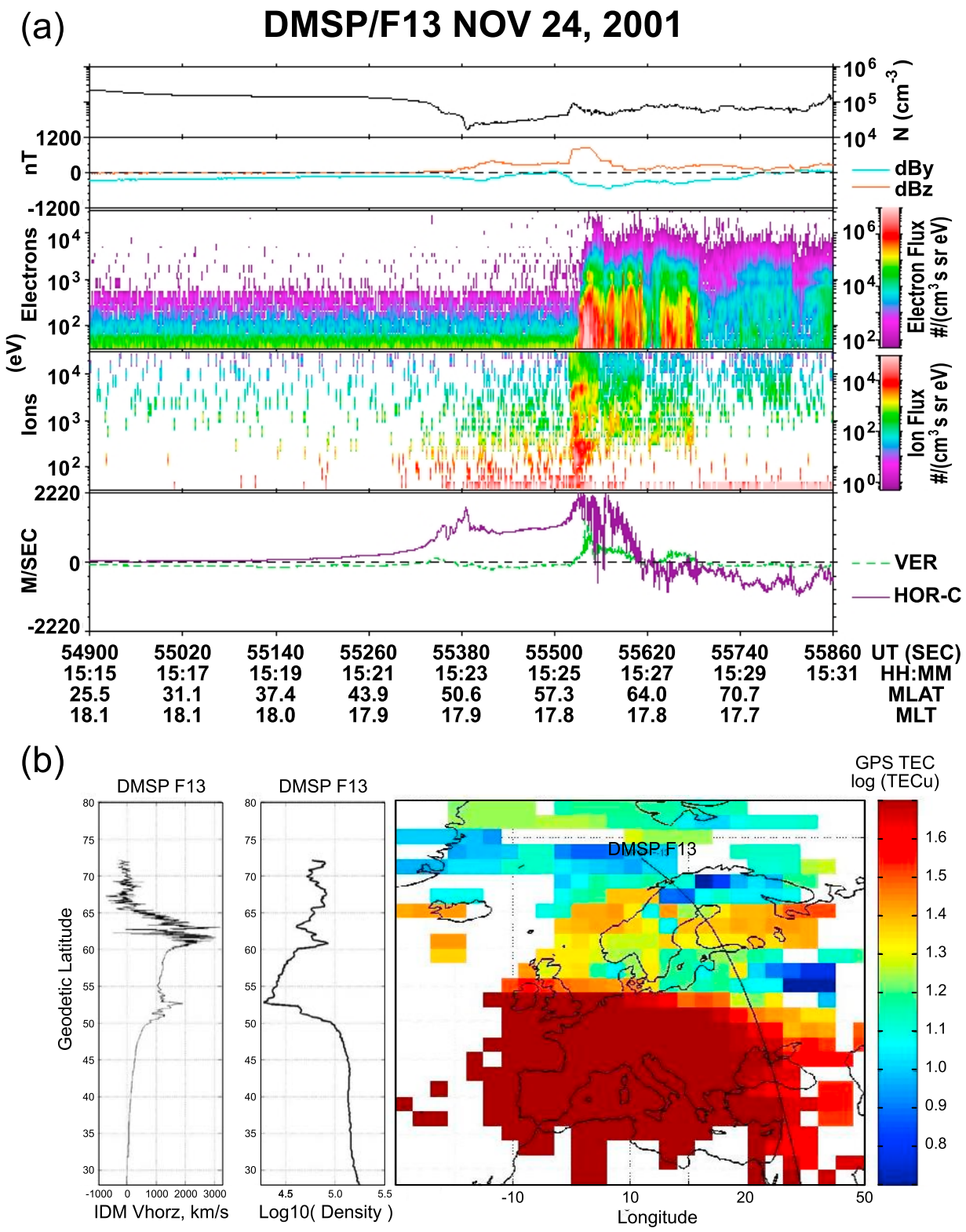

Figure 13. SAPS flows and density structuring. (a) Data from the DMSP/F13 spacecraft between 1515 and 1531 UTC on 24 November 2001. Shown are electron density, magnetic field perturbations, energy versus time spectrogram for precipitating electron flux, energy versus time spectrogram for precipitating proton flux, and the vertical (green) and horizontal cross-track (purple) ion flow velocities. Note the elevated horizontal cross-track flows that exist well equatorward of the precipitating electron region. (b) GPS total electron content (TEC) measurements over Scandinavia at 1520 UTC. Enhanced, spatially structured density is observed in the regions where the GUs are located. The DMSP/F13 track is overplotted, and the horizontal flow velocity and electron density are also replotted in a different format.

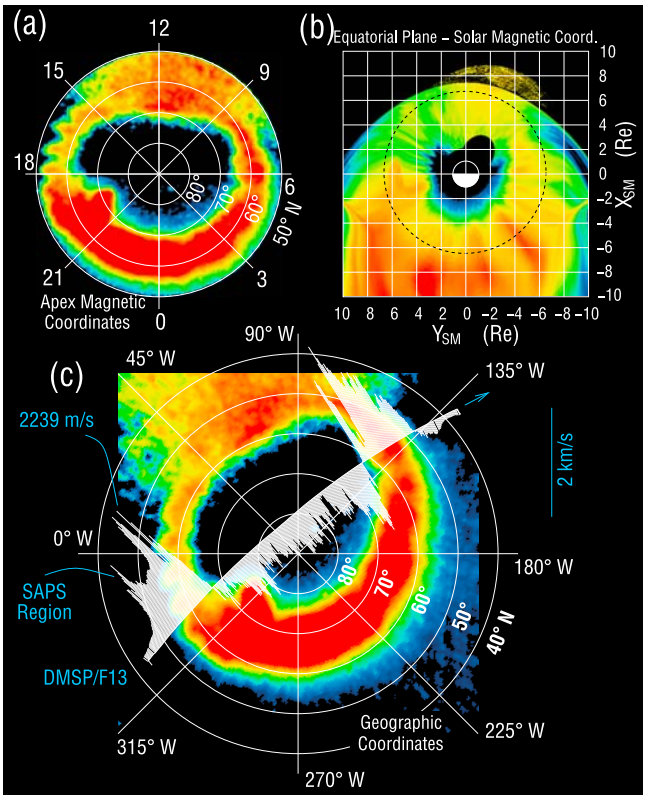

Figure 14. (a) FUV image taken at 1525:41 UTC with Apex magnetic coordinate grid overlaid. (b) The image shown in Figure 14a, mapped to the equatorial plane of the SM coordinate system. The dynamic TS04 model was used. (c) The 1525:41 UTC FUV image in geographic coordinates with the DMSP/F13 cross-track plasma drift vectors overlayed. The trajectory of DMSP has been mapped down the field lines to the foot point at 120 km altitude using the T89 K_p = 5 model with IGRF internal field model.

field line which is typically found near the equatorial plane). Figure 14a, therefore, shows that the undulations map slightly closer to the Earth near dusk than they do in the post noon sector, and this is also shown (although not as clearly) in Figure 14b. The dashed black circle in Figure 14b represents geosynchronous orbit, which at this time approaches close to the model magnetopause on the dayside. The giant undulations can be seen extending from the postdusk sector to the afternoon sector and their inner edges map as close to the Earth as approximately $3R_E$ on the duskside. (Note that some of the boundaries associated with the inner edge, especially in the 06–15 MLT range, are artificial because of the truncation of the auroral image data at 50°N MLAT.) Finally, in Figure 14c, we present the 1525:41 UTC FUV/WIC image in geographic coordinates with the DMSP/F13 ion horizontal drift vectors overlayed along the spacecraft trajectory, which has been mapped down magnetic field lines to an altitude of 120 km. One can immediately see that the SAPS region (near 50°N geographic latitude) is closely coincident with the equatorward edge of the giant undulation region seen in the image.

[28] The magnitude of the SAPS flows from DMSP 13, 14, and 15 in the 18–21 MLT sector from 1100–1800 UTC on 24 November 2001 is shown in Figure 15. As can be seen from this plot, the SAPS flows are elevated between approximately 1300–1600 UTC. The darker blue-shaded region drawn between 1344 and 1600 UTC represents the time period during which giant undulations can be seen in the IMAGE FUV data. And the lighter blue-shaded region represents the time period prior to this during which structuring of the equatorward edge of the diffuse aurora could be seen in the DMSP OLS imager data (see Figure 12a). We note that the combined time period is very closely associated with the time during which enhanced SAPS flows were seen in the 18–21 MLT sector. This provides strong evidence that the formation of the GUs may in fact be causally related to the onset of strong SAPS flows. And that their subsidence is caused by the reduction of the SAPS flows to lower levels.

3. Discussion

[29] In this paper, we have presented high time resolution, start-to-finish global auroral imaging of a giant auroral undulation event. The undulations developed near the peak of an intense geomagnetic storm during an interval of very high convection (as indicated by large values of the K_p index) and lasted for more than 2 h. These observations are consistent with previous studies that showed GUs existing under similar conditions and at similar times relative to the storm phase [e.g., *Lui et al.*, 1982]. The GUs observed here had a wavelength of ~718 km and amplitudes of ~890 km and were observed to propagate systematically sunward with a phase speed of ~0.6 km/s. The sunward speed is comparable to the results of *Nishitani et al.* [1994], but the undulations observed here were much larger in size.

[30] The undulations developed on the duskside about 1 h after the onset of an intense substorm. This association with prior substorm activity is consistent with the results of

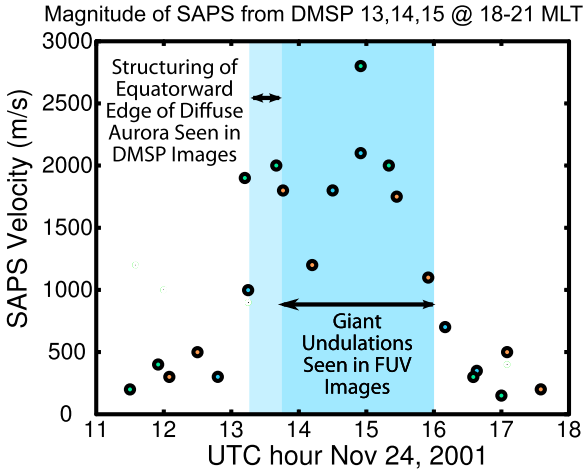

Figure 15. SAPS velocity in the 18–21 MLT sector versus time as measured with DMSP F13, F14, and F15. The darker blue shading indicates the time period during which giant undulations were seen in IMAGE/FUV data. The lighter blue shading indicates the time period during which structuring of the equatorward edge of the diffuse aurora was seen in the DMSP/OLS data. The combined time period is closely coincident with the elevated SAPS flows.

Baishev et al. [2000]. However, in our case, the undulations also developed in close temporal proximity to a solar wind pressure pulse that globally intensified the northern auroral emissions. It is, therefore, unclear what caused the undulations to develop, but we speculate that prior substorm injection activity, which produces transient azimuthal pressure gradients in the inner magnetosphere, may be a necessary condition for undulations to develop. Nevertheless, such preconditioning is obviously not a sufficient condition since GUs are not observed in conjunction with every substorm. The final subsidence of the GU waveform more than 2 h after its development, occurred about an hour after the IMF turned northward and was associated with: a subsidence of the SAPS flows in the 18–21 MLT sector, a global fading of the auroral distribution and a relaxation of the SW pressure impinging on the Earth.

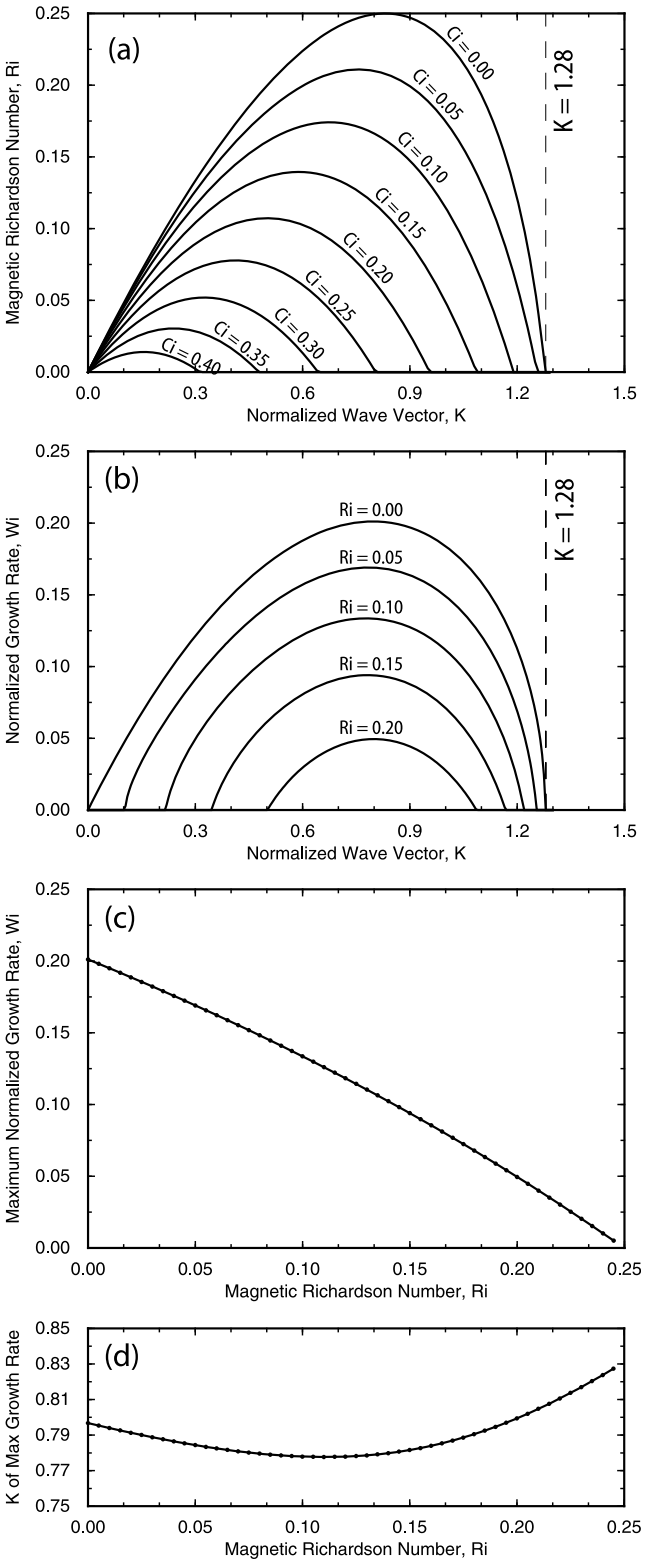

Figure 16. Unstable solutions to the dispersion relation [*Vinas and Madden*, 1986, equation (37)]. (a) Magnetic Richardson number as a function of normalized wave vector for various values of the normalized phase speed. (b) Normalized growth rate as a function of normalized wave vector for various values of magnetic Richardson number. (c) Maximum normalized growth rate as a function of magnetic Richardson number. (d) Value of normalized wave vector at maximum normalized growth rate.

[31] We have also shown that the GUs developed in a region adjacent to a pronounced SAPS flow and that the latitudinal range occupied by the GUs was colocated with a band of spatially structured density near the plasmapause in the region that one might refer to as the plasmaspheric boundary layer [*Carpenter and Lemaire*, 2004]. On the basis of comparisons between POLAR/VIS N_2^+ 391.4 nm and OI 630.0 nm auroral images, we surmise that the SAPS was produced as a consequence of the proton plasma sheet penetrating earthward of the electron plasma sheet on the duskside. In such a configuration, large poleward electric fields will develop in the subauroral region (i.e., equatorward of the electron aurora), because ionospheric currents must flow through regions of very low conductance (to maintain the current, the *E* field must increase). This electric field also maps into the magnetosphere and produces a channel of strongly enhanced sunward convection [e.g., *Foster and Burke*, 2002; *Foster and Vo*, 2002; *Foster et al.*, 2004].

[32] Together, these observations suggest that the giant undulations may have been produced as a result of a Kelvin-Helmholtz/interchange instability because of the intense sheared flow near the equatorward edge of the diffuse electron aurora as has been suggested previously by *Vinas and Madden* [1986], *Kelley* [1986], and *Murphree and Johnson* [1996]. Under certain approximations, *Vinas and Madden* [1986] showed that a sufficient condition for the development of this "shear-flow-ballooning" instability is that

$$R_i = \frac{\left[\Omega_g^2(r) + k_\parallel^2 C_\mathrm{A}^2\right]\left(1 + k_\parallel^2/k_\perp^2\right)}{\left(\partial V_\phi/\partial r\right)^2} < \frac{1}{4}, \qquad (1)$$

where R_i is the (dimensionless) "local magnetic Richardson number," Ω_g is the magnetic Brunt-Väisälä (BV) frequency (also called the interchange or Rayleigh-Taylor frequency), C_A is the Alfven speed, $\partial V_\phi/\partial r$ is the velocity shear, and $k_\parallel$ and $k_\perp$ are the parallel and perpendicular components of the wave vector. Note that, although the interchange instability grows when the quantity $\Omega_g^2(r) + k_\parallel^2 C_a^2$ becomes negative, this will never happen before R_i becomes less than 1/4 (because when $\Omega_g^2(r) + k_\parallel^2 C_a^2$ approaches 0, even vanishingly small

values of the velocity shear can result in $R_i < 1/4$). Thus, as pointed out by *Vinas and Madden* [1986], this appears to indicate that the interchange instability cannot occur before the shear flow instability.

[33] We have recomputed solutions to the dispersion relation (for $k_{\|} \ll k_{\perp}$) derived by *Vinas and Madden* [1986, equation (37)], and the results are shown in Figure 16. Figure 16a shows the magnetic Richardson number as a function of the normalized wave vector for a variety of values of the normalized imaginary phase velocity (here the normalized real part of the phase velocity is fixed at 0.5, which is a consequence of the symmetry in the plasmapause model chosen by *Vinas and Madden* [1986]). Figure 16b shows the normalized growth rate as a function of the normalized wave vector for a variety of values the magnetic Richardson number. Figures 16c and 16d show the maximum normalized growth rate and the value of K at which it occurs as a function of magnetic Richardson number. From Figures 16a and 16b, we can see that there is an upper cutoff for the normalized wave vector (equal to 1.28). From this, we can derive a crude estimate of the maximum m number for the waves as

$$m_{\max} = \frac{K_{\max} L_{\mathrm{pp}}}{\Delta}, \tag{2}$$

where Δ is the scale length (in units of Earth radii) of the velocity shear and L_{pp} is the position of the plasmapause (also in units of Earth radii). If we take $\Delta = 0.15\ R_E$ [see, e.g., *Vinas and Madden*, 1986], and $L_{\mathrm{pp}} = 4.0\ R_{\mathrm{E}}$, then $m_{\max} \approx 34$, and this is consistent with the m number found for the event studied here, which was about 32.

[34] It is important to note that *Vinas and Madden* [1986] derived the aforementioned instability condition using a number of physical assumptions. They neglected kinetic effects and they assumed an isotropic pressure. But, perhaps more importantly, they ignored the so-called "line-tying" effect [e.g., *Kunkel and Guillory*, 1966; *Guest and Beasley*, 1966; *Prater*, 1974] in which the motion of the ionospheric feet of field lines is impeded by finite conductivity effects. Since the line-tying effect tends to stabilize the interchange instability, interchange is difficult to achieve in the auroral zone (or on the dayside), where the conductivity is high. However, as we have seen, the SAPS-induced shear flow associated with the undulations occurs in (indeed is a consequence of) a region of low ionospheric conductivity which is precisely where the stabilizing effects of line tying should be minimized.

[35] An additional approximation used by *Vinas and Madden* [1986] is the so-called "Boussinesq approximation." In this approximation, all density gradient terms are ignored except those that contribute to the Buoyancy force. In subsequent studies, *Satyanarayana and Lee* [1987] and *Wang and Pritchett* [1989] have also examined the stability of a compressible stratified shear layer, and by relaxing the Boussinesq approximation, they conclude that the "critical Richardson number" is not a constant value of 1/4. Instead, they find that it depends on β, the ratio of the velocity scale length to the density gradient scale length ($\beta = L_v/L_n$) and on the details of the magnetic field configuration. In the *Satyanarayana and Lee* [1987] results, they find that when $\beta > 2$, the Kelvin-Helmholtz instability is stable and that the system is unstable only when the R_i becomes negative (i.e., when the ballooning/interchange mode grows). In addition, they find that the critical Richardson number becomes quite small when the density gradient is steep at the plasmapause and they conclude that strong shears at the plasmapause may not drive the shear flow ballooning instability as described by *Vinas and Madden* [1986]. On the other hand, *Wang and Pritchett* [1989] showed that the *Satyanarayana and Lee* [1987] results are not valid in general. Thus, the value of the critical Richardson number and its dependence on the β parameter is still an open question.

[36] *Lakhina et al.* [1990] point out further problems with the instability analysis of *Vinas and Madden* [1986]. These include: (1) the assumption of circular field lines (i.e., no radial component of the B field); (2) restriction to local stability analysis only; and (3) an apparent violation of the assumption that $|\omega^2 - k_{\|}^2 c_a^2| \ll |\Omega^2|$. *Lakhina et al.* [1990] derive a more general stability criterion that should probably be used in future studies of giant undulations. A general conclusion they arrive at is that the presence of shear at the plasmapause tends to reinforce the stability or instability of the plasmapause to ballooning modes. In other words, if the plasmapause is already unstable to the growth of ballooning modes, shear will make these modes more unstable and if the plasmapause is already stable to the growth of ballooning modes, shear will make the system even more stable to the growth of ballooning modes.

[37] The shear flow ballooning instability of *Vinas and Madden* [1986] generates ULF pulsations in the Pc4–Pc6 range. From their nominal plasmapause model parameters, they predict ULF pulsations with periods in the 131–348 s range. The pulsations observed during the 24 November 2001 event presented here have somewhat longer periods (approximately 1100 s) than this, but we note that most of the parameters involved in computing the frequency properly are in reality not well known. For example, the symmetry of the model by *Vinas and Madden* [1986] leads to a constant normalized real part of the phase velocity of 0.5, and this is used to compute the ULF pulsation frequencies. In addition, extremely simple functional forms were used for the density, temperature, and velocity profiles across the shear zone. For more realistic and better specified plasmapause models, (as well as dropping the Boussinesq approximation) it is may be that our observed ULF frequency could be generated by this mechanism. However, the numerous shortcomings of the theory (as discussed earlier) need to be resolved before a more definitive statement regarding its consistency with observations can be made.

[38] Other physical mechanisms for the generation of ripples, undulations and giant undulations at the equatorward edge of the diffuse aurora have been proposed. Assuming the existence of an "arc sheet" (their name for a polarization jet or SAPS-like feature) *Yamamoto et al.* [1991] showed that undulations could develop in a two-dimensional electrostatic particle simulation as a result of the velocity-shear-induced Kelvin-Helmholtz instability. However, *Yamamoto et al.* [1993, 1994] found that large-amplitude, "giant undulations" (amplitude comparable with wavelength) could not be produced with a single polarization jet alone. Instead, they proposed a model in which an initial "arc sheet" can become

polarized via anomalous cross-field diffusion of the protons resulting in a region of net negative space charge sandwiched between two regions of net positive space charge. They showed that this type of configuration could lead to giant undulations. Although the development of KHI is consistent with the results of *Vinas and Madden* [1986], these simulations neglected compressibility effects and so interchange modes were ignored.

[39] In a more recent study, *Sazykin et al.* [2002] find that in an improved version of the Rice convection model (RCM), an interchange-like instability can develop in the dusk-to-midnight sector and produce undulations near the equatorward edge of the diffuse aurora. The instability appears to proceed as a result of earthward propagation of low-entropy (low-PV^{γ}) flux tubes that are in turn introduced into the model domain as large and sustained decreases in the value of PV^{γ} at the boundary of the simulation (i.e., at geosynchronous orbit). The resulting layer of depleted (low PV^{γ}) flux tubes outside (i.e., farther from the Earth) a region of flux tubes with higher values of PV^{γ}, is naturally interchange unstable provided that the flux tube volume increases monotonically as one moves away from the Earth (which is true in the inner magnetosphere). The simulation results show that as the instability develops, fingers of low-PV^{γ} flux tubes penetrate inward while fingers of high-PV^{γ} flux tubes move outward. The adiabatic deenergization of the outward moving high-PV^{γ} flux tubes is expected to lead to a sudden reduction in the particle energy of the ring current and a concomitant reduction in the D_{st} index.

[40] In this paper, we do not observe a sudden recovery in the D_{st} index in association with the development of the giant undulations. In addition, the undulations seen here (and during a number of other events) extend well past the (sunwardside of the) 18 MLT meridian. Although our observations do not appear to be consistent with the results of *Sazykin et al.* [2002], the mechanism they describe may nevertheless contribute to the destabilization of the inner magnetosphere to interchange modes. It is also interesting to note that their mechanism may also be related to one proposed by *Henderson et al.* [2002] in terms of Ω band formation via flow bursts. As shown by *Henderson et al.* [2002], auroral torches and omega bands can be produced by equatorward moving auroral streamers which are thought to be signatures of earthward moving flow bursts in the tail [e.g., *Henderson et al.*, 1994, 1998; *Zesta et al.*, 2000]. Since a likely mechanism for flow bursts is the earthward penetration of localized depleted flux tubes [*Chen and Wolf*, 1993] (produced, for example, by patchy and/or intermittent reconnection in the tail), the mechanism proposed by *Sazykin et al.* [2002] may be more relevant for the production of Ω bands than for the production of duskside GUs. In addition, the large and sustained decreases in flux tube content leading to interchange in the results of *Sazykin et al.* [2002] may be able to explain the large-scale deformations in the plasmapause commonly seen to develop in the recovery phase of storms.

[41] Finally, we note that while the equatorward edge of the auroral distribution is usually quite sharp, during disturbed times it can become quite structured and complex. Although a detailed examination of such events is beyond the scope of this paper, we speculate that nonlinear growth of an instability like the shear flow ballooning instability could result in significant plasma mixing within the shear zone.

4. Conclusions

[42] The giant undulations observed during the 24 November 2001 event had wavelengths of ~718 km and amplitudes of ~890 km and were observed to propagate sunward with a phase speed of ~0.6 km/s. The giant undulations appear to be associated with intense substorm activity, but we also find evidence that pressure pulses could have played a role as well. The undulations were also associated with very long period ULF pulsations ($T \approx 1108$ s).

[43] We have shown that the giant undulations were associated with SAPS flows that were likely caused by the proton plasma sheet penetrating substantially farther earthward than the electron plasma sheet on the duskside. We suggest that the observations are approximately consistent with the development of a shear flow ballooning type of instability of the type proposed by *Vinas and Madden* [1986].

[44] **Acknowledgments.** The research at Los Alamos National Laboratory was supported by NSF GEM grant ATM-0202303. The SAMNET is operated by the Department of Communications Systems at Lancaster University, United Kingdom, and is funded by the Science and Technology Facilities Council. The Sym-H index data were provided by the World Data Center for Geomagnetism at Kyoto University. The polar magnetic field data were obtained via the UCLA online data server, and we thank C. Russell for making these data available there. We would also like to acknowledge the efforts of R. Skoug in providing us with corrected ACE solar wind data. M.G.H. points out that much of the contents of this paper was first presented at the fall 2002 AGU meeting and apologizes to coauthors for taking so long to publish the results.

[45] Amitava Bhattacharjee thanks Evgeny Mishin and another reviewer for their assistance in evaluating this paper.

References

Baishev, D. G., E. S. Barkova, S. I. Solovyev, K. Yumoto, M. J. Engebretson, and A. V. Koustov (2000), Formation of large-scale giant undulations at the equatorial boundary of diffuse aurora and Pc5 magnetic pulsations during the January 14, 1999 magnetic storm, in *Proceedings of the Fifth International Conference on Substorms*, edited by A. Wilson, *Eur. Space Agency Spec. Publ., ESA SP-443*, 427–430.

Carpenter, D. L., and J. Lemaire (2004), The plasmasphere boundary layer, *Ann. Geophys.*, *22*, 4291–4298.

Chen, C. X., and R. A. Wolf (1993), Interpretation of high speed flows in the plasma sheet, *J. Gephys. Res.*, *98*, 21,409–21,419.

Coster, A. J., J. C. Foster, and P. J. Erickson (2003), Monitoring the ionosphere with GPS, *GPS World*, *14*(5), 42–49.

Foster, J. C., and W. J. Burke (2002), SAPS: A new characterization for sub-auroral electric fields, *Eos Trans. AGU*, *83*(36), 393, doi:10.1029/2002EO000289.

Foster, J. C., and H. B. Vo (2002), Average characteristics and activity dependence of the subauroral polarization stream, *J. Geophys. Res.*, *107*(A12), 1475, doi:10.1029/2002JA009409.

Foster, J. C., P. J. Erickson, A. J. Coster, J. Goldstein, and F. J. Rich (2002), Ionospheric signatures of plasmaspheric tails, *Geophys. Res. Lett.*, *29*(13), 1623, doi:10.1029/2002GL015067.

Foster, J. C., A. J. Coster, P. J. Erickson, F. J. Rich, and B. R. Sandel (2004), Stormtime observations of the flux of plasmaspheric ions to the dayside cusp/magnetopause, *Geophys. Res. Lett.*, *31*, L08809, doi:10.1029/2004GL020082.

Fuselier, S. A., H. L. Collin, A. G. Ghielmetti, E. S. Claflin, T. E. Moore, M. R. Collier, H. Frey, and S. B. Mende (2002), Localized ion outflow in response to a solar wind pressure pulse, *J. Geophys. Res.*, *107*(A8), 1203, doi:10.1029/2001JA000297.

Goldstein, J., J. L. Burch, and B. R. Sandel (2005), Magnetospheric model of subauroral polarization stream, *J. Geophys. Res.*, *110*, A09222, doi:10.1029/2005JA011135.

Guest, G. E., and C. Beasley Jr. (1966), Cold-plasma effects in finite-length plasmas, *Phys. Fluids*, *9*, 1798–1804.

Henderson, M. G., J. S. Murphree, and G. D. Reeves (1994), The activation of the dusk-side and the formation of north-south aligned structures during substorms, in *Proceedings of Second International Conference on Substorms (ICS-2)*, edited by J. R. Kan, J. D. Craven, and S.-I. Akasofu, p. 37, Geophys. Inst., Univ. of Alaska Fairbanks, Fairbanks.

Henderson, M. G., G. D. Reeves, and J. S. Murphree (1998), Are north-south aligned auroral structures an ionospheric manifestation of bursty bulk flows?, *Geophys. Res. Lett.*, *25*, 3737–3740.

Henderson, M. G., L. Kepko, H. E. Spence, M. Connors, J. B. Sigwarth, L. A. Frank, H. J. Singer, and K. Yumoto (2002), The evolution of north-south aligned auroral forms into auroral torch structures: The generation of omega bands and Ps6 pulsations via flow bursts, in *Proceedings of the Sixth International Conference on Substorms*, edited by R. M. Winglee, pp. 169–174, Univ. of Wash., Seattle.

Immel, T. J., S. B. Mende, H. U. Frey, L. M. Peticolas, C. W. Carlson, J.-C. Gérard, B. Hubert, S. A. Fuselier, and J. L. Burch (2002), Precipitation of auroral protons in detached arcs, *Geophys. Res. Lett.*, *29*(11), 1519, doi:10.1029/2001GL013847.

Kelley, M. C. (1986), Intense sheared flow as the origin of large-scale undulations of the edge of the diffuse aurora, *J. Geophys. Res.*, *91*, 3225–3230.

Kunkel, W. B., and J. U. Guillory (1966), Interchange stabilization by incomplete line-tying, in *Phenomena in Ionized Gases*, vol. II, *Plasma Physics, Proceedings of the Seventh International Conference*, pp. 702–706, Gradevinska Knjiga, Belgrade, Yugoslavia.

Lakhina, G. S., M. Mond, and E. Hameiri (1990), Ballooning mode instability at the plasmapause, *J. Geophys. Res.*, *95*, 4007–4016.

Lin, C. S., H.-C. Yeh, B. R. Sandel, J. Goldstein, F. J. Rich, W. J. Burke, and J. C. Foster (2007), Magnetospheric convection near a drainage plume, *J. Geophys. Res.*, *112*, A05216, doi:10.1029/2006JA011819.

Lui, A. T. Y., C. I. Meng, and S. Ismail (1982), Large amplitude undulations on the equatorward boundary of the diffuse aurora, *J. Geophys. Res.*, *87*, 2385–2400.

Lummerzheim, D., M. Galand, J. Semeter, M. J. Mendillo, M. H. Rees, and F. Rich (2001), Emission of OI (630 nm) in proton aurora, *J. Geophys. Res.*, *106*, 141–148.

Mendillo, M., J. Baumgardner, and J. Providakes (1989), Ground based imaging of detached arcs, ripples in the diffuse aurora, and patches of 6300Å emission, *J. Geophys. Res.*, *94*, 5367–5381.

Mishin, E. V., and W. J. Burke (2005), Stormtime coupling of the ring current, plasmasphere, and topside ionosphere: Electromagnetic and plasma disturbances, *J. Geophys. Res.*, *110*, A07209, doi:10.1029/2005JA011021.

Mishin, E. V., and V. M. Mishin (2007), Prompt response of SAPS to stormtime substorms, *J. Atmos. Sol. Terr. Phys.*, *69*, 1233–1240.

Murphree, J. S., and M. L. Johnson (1996), Clues to plasma processes based on Freja UV observations, *Adv. Space Res.*, *18*, 95–105.

Nishitani, N., G. Hough, and M. W. J. Scourfield (1994), Spatial and temporal characteristics of giant undulations, *Geophys. Res. Lett.*, *21*, 2673–2676.

Prater, R. (1974), Interchange destabilization by incomplete line-tying, *Phys. Fluids*, *17*, 193–197.

Provadakes, J. F., M. C. Kelley, W. E. Swartz, and M. Mendillo (1989), Radar and optical measurements of ionospheric processes associated with intense subauroral electric fields, *J. Geophys. Res.*, *94*, 5350–5366.

Rideout, W., and J. C. Foster (2005), Midlatitude TEC enhancements during the October 2003 superstorm, *Geophys. Res. Lett.*, *32*, L12S04, doi:10.1029/2004GL021719.

Satyanarayana, P., and Y. C. Lee (1987), The stability of a stratified shear-layer, *Phys. Fluids*, *30*, 81–83.

Sazykin, S., R. A. Wolf, R. W. Spiro, T. I. Gombosi, D. L. De Zeeuw, and M. F. Thomsen (2002), Interchange instability in the inner magnetosphere associated with geosynchronous particle flux decreases, *Geophys. Res. Lett.*, *29*(10), 1448, doi:10.1029/2001GL014416. (Correction, *Geophys. Res. Lett.*, *31*, L05803, doi:10.1029/2003GL019191, 2004.)

Tsyganenko, N. A., and M. I. Sitnov (2005), Modeling the dynamics of the inner magnetosphere during strong geomagnetic storms, *J. Geophys. Res.*, *110*, A03208, doi:10.1029/2004JA010798.

Vinas, A. F., and T. R. Madden (1986), Shear flow–ballooning instability as a possible mechanism for hydromagnetic fluctuations, *J. Geophys. Res.*, *91*, 1519–1528.

Wang, Z., and P. L. Pritchett (1989), The stability of a compressible stratified shear layer, *Phys. Fluids B*, *1*, 1767–1775.

Yamamoto, T., K. Makita, and C.-I. Meng (1991), A particle simulation of large-amplitude undulations on the evening diffuse auroral boundary, *J. Geophys. Res.*, *96*, 1439–1449.

Yamamoto, T., K. Makita, and C.-I. Meng (1993), A particle simulation of "giant" undulations on the evening diffuse auroral boundary, *J. Geophys. Res.*, *98*, 5785–5800.

Yamamoto, T., M. Ozaki, S. Inoue, K. Makita, and C.-I. Meng (1994), Convective generation of "giant" undulations on the evening diffuse auroral boundary, *J. Geophys. Res.*, *99*, 19,499–19,512.

Zesta, E., L. R. Lyons, and E. Donovan (2000), The auroral signature of earthward flow bursts observed in the magnetotail, *Geophys. Res. Lett.*, *27*, 3241–3244.

E. F. Donovan, Department of Physics and Astronomy, University of Calgary, 2500 University Dr. NW, Calgary, AB T2N 1N4, Canada.

J. C. Foster, Haystack Observatory, Massachusetts Institute of Technology, Rte. 40, Westford, MA 01886-1299, USA.

M. G. Henderson, Los Alamos National Laboratory, ISR-1, MS-D466, Los Alamos, NM 87544, USA. (mghenderson@lanl.gov)

T. J. Immel and S. B. Mende, Space Sciences Laboratory, University of California, Berkeley, CA 94720, USA.

I. R. Mann, Department of Physics, University of Alberta, Edmonton, AB T6G 2G2, Canada.

J. B. Sigwarth, NASA Goddard Space Flight Center, Greenbelt, MD 20770, USA.